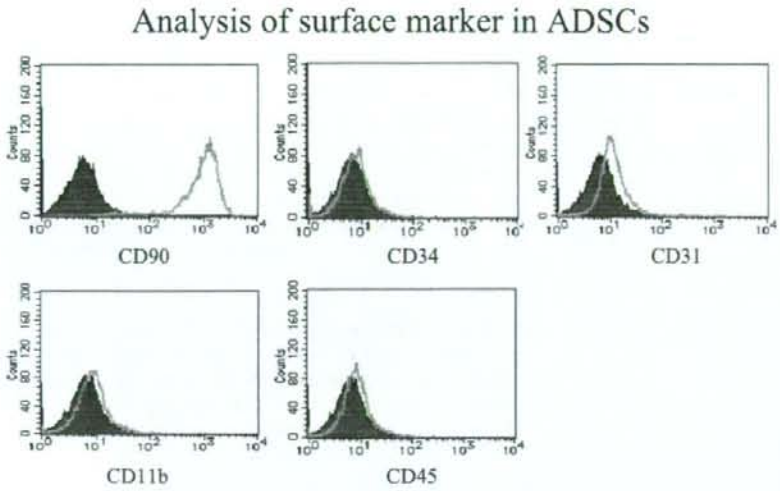

FIGURE 2. Characterization of ADSCs. ADSCs (passage 3) were flow-cytometrically characterized using antibodies against CD11b, CD31, CD34, CD45, and CD90. Cells stained with mAbs are represented by solid pink lines, and those stained with isotype-matched Ig, as negative controls, are represented by green lines. Cells were negative for CD11b, CD34, and CD45 but positive for CD90 and weakly positive for CD31.

Mann-Whitney test. The statistical analysis for the survival rate was performed by log rank test. A P value less than .05 was considered statistically significant. The experimental protocol was approved by the Ethics Review Committee for Animal Experimentation of Kansai Medical University.

RESULTS

Characterization of ADSCs from Subcutaneous Adipose Tissue

ADSCs were flow-cytometrically characterized (after 3 passages) and possible contaminants of hemopoietic lineage cells were excluded. ADSCs were negative for CD11b, CD34, and CD45 but positive for CD90 as shown in Figure 2, indicating that the ADSCs used in our experiments are not in the hemopoietic cell lineages. It is noted that a slight shift in the entire histogram was observed after staining with anti-CD31, indicating that ADSCs seem to be weakly positive for CD31. Furthermore, the doubling time of ADSCs remained unchanged (approximately 36–40 hours) up to 10 passages (Fig. 3). However, their growth stopped at 15 passages.

ADSCs Exhibit Multilineage Potential

We next examined the capacity of ADSCs to differentiate into multilineage cells under the appropriate culture conditions. ADSCs differentiated into adipocytes, osteocytes, neu-

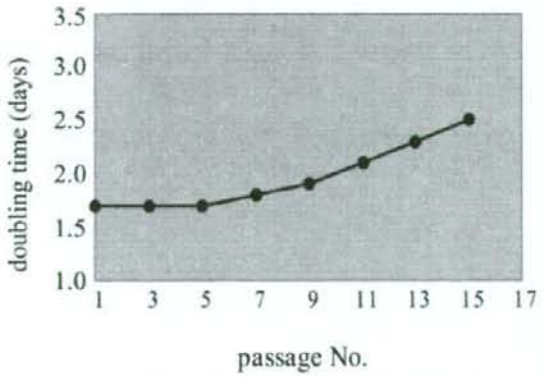

FIGURE 3. Doubling time of ADSCs. Doubling time (day) of ADSCs was determined at the indicated number of passages in DMEM.

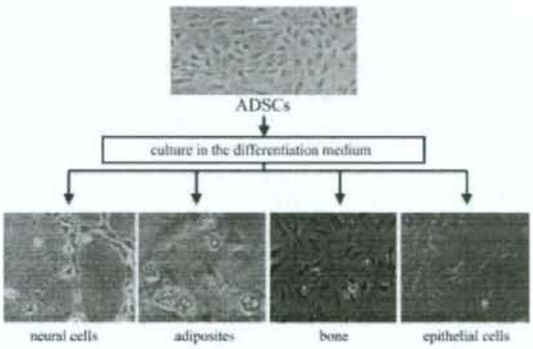

FIGURE 4. Culture of ADSCs. Multilineage differentiation was observed in the appropriate culture condition (bottom). Undifferentiated ADSCs showed multiple layers in the control culture medium.

rogenic cells, and epithelial cells using lineage-specific induction factors. Undifferentiated ADSCs cultured in the medium alone showed multiple layers. Neurogenic differentiation was confirmed by the expression of NSE in the cells with a neuronal morphology (Figs. 4 and 5), and adipogenesis was examined by Oil Red-O staining (Figs. 4 and 5). No lipid droplets stainable with Oil Red-O were observed in undifferentiated ADSCs. Differentiation toward osteocytes was determined by calcification of the extracellular matrix using von Kossa/alkaline phosphatase staining. ADSCs cultured in the epitheliogenic condition (5 μM ATRA for 10 days) showed a morphology resembling epithelial cells (Fig. 4), and they

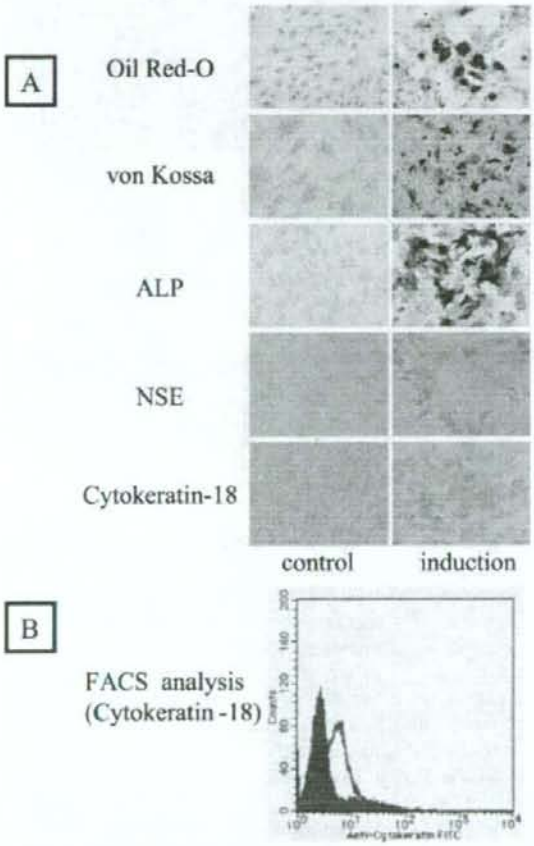

FIGURE 5. Immunohistochemical analyses of ADSCs after differentiation. ADSCs were cultured for 2–4 weeks in adipogenic, osteogenic, neurogenic, or epitheliogenic medium. A: ADSCs thus cultured were stained with Oil Red-O, von Kossa, alkaline phosphatase, NSE, or cytokeratin-18 to identify their differentiation. B: ADSCs cultured with epitheliogenic medium were flow-cytometrically analyzed after staining with FITC-anti-cytokeratin-18 mAb.

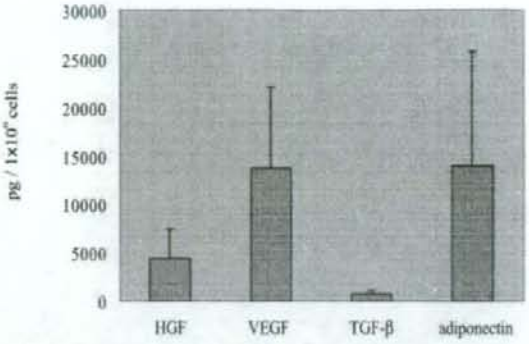

FIGURE 6. Secretion of HGF, VEGF, TGF-β and adiponectin by ADSCs. ADSCs were cultured for 1 week, and the amounts of HGF, VEGF, TGF-β, and adiponectin were measured by ELISA. Columns and bars represent the means ± SDs of 14 samples.

were positive for cytokeratin 18 as shown in Figure 5, where a filamentous cytoskeleton, the typical appearance of epithelial cytokeratins, was stained with this mAb. This was flow-cytometrically confirmed after staining with FITC-anti-cytokeratin-18 mAb (Fig. 5B).

ADSCs Secrete VEGF, HGF, TGF-β, and Adiponectin

The secretion of HGF, VEGF, TGF-β , and adiponectin from ADSCs was examined. They secreted significant amounts of VEGF (13,654 ± 3185 pg/10^6 cells), HGF (4434 ± 1140 pg/10^6 cells), and adiponectin (13,910 ± 5902 pg/10^6 cells) but only minimal amounts (733 ± 136 pg/10^6 cells) of TGF-β (Fig. 6).

Inoculation of ADSCs Reduces Severity of TNBS-Induced Colitis

Changes in body weight, colon weight, and survival rate were evaluated for assessment of the severity of colitis (Fig. 7). There was no statistical significance in the changes in body weight or survival rate between the recipients of ADSCs and the recipients of PBS in TNBS-induced colitis-model rats. However, a significant decrease in colonic weight was observed in the recipients submucosally injected with ADSCs, suggesting that the colonic edema associated with inflammatory responses was ameliorated by the inoculation of ADSCs. Although the results shown in Figure 7 represent only 2 replicate experiments, the values and outcomes in the other experiment were similar to those in Figure 7.

Inoculation of ADSCs Facilitates Repair of Colonic Ulcers

Next, we examined the effects of ADSCs on the repair of colonic ulcers. Eight days after the submucosal injection of ADSCs (or PBS), rats were sacrificed, and the area of colonic

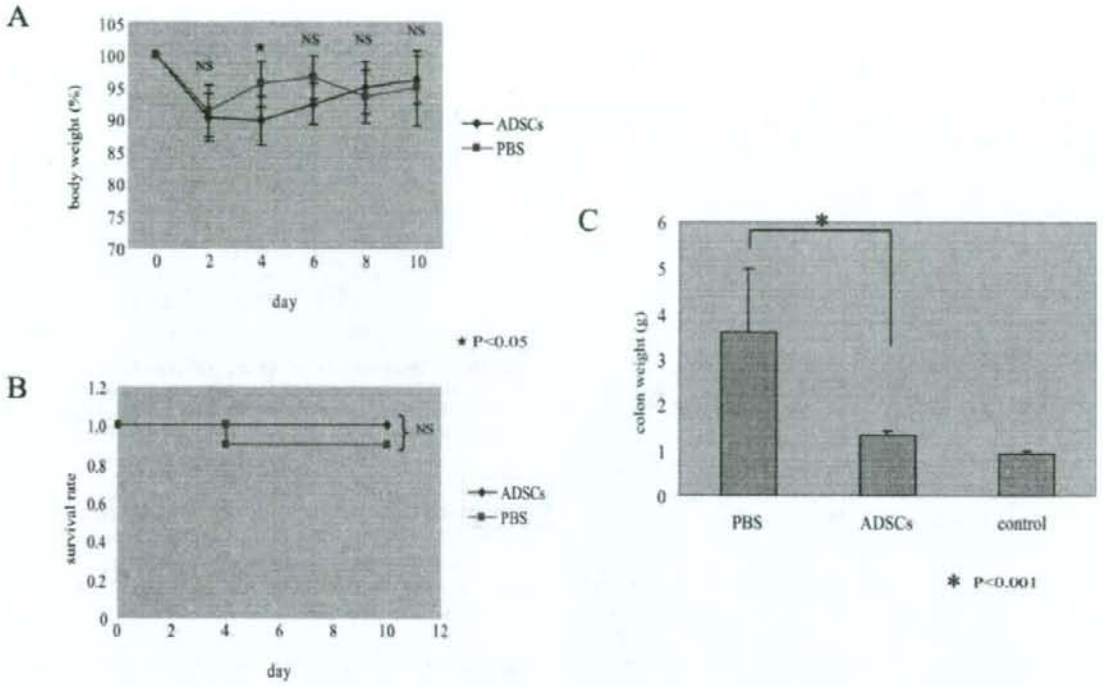

FIGURE 7. Measurement of body and colonic weight and survival rate after inoculating the colitis-model rats with ADSCs. A: Body weight was measured every 2 days, and colonic weight was determined 8 days after the injection of ADSCs (10 days after the injection of TNBS). It is noted that there was no statistically significance difference in body weight between the recipients of PBS and the recipients of ADSCs (except on day 4). B: Effects of ADSCs on survival rate were examined. Statistical analysis was performed by the log rank test. C: Colonic weight was measured 8 days after the submucosal injection of ADSCs. The results are representative of 2 replicate experiments. Symbols, columns, and bars represent the means ± SDs of 10 rats ($^*P < 0.001$).

ulcers and colon length were measured (Fig. 8A). As shown in Figure 8B, the ulcer area was significantly reduced (23 ± 2 mm^2) in the TBNS-induced-colitis rats treated with ADSCs compared with those treated with PBS (65 ± 13 mm^2; $P < 0.05$). However, there was no statistically significant difference in colonic length between the rats treated with ADSCs (15.2 ± 0.2 cm) and the rats treated with PBS (15.3 ± 0.8 cm; Fig. 8C). Furthermore, we evaluated the proliferation of colonic epithelium (photographed in Fig. 8D,E) by the injection of BrdU. When the colitis-induced rats were treated with ADSCs, the number of BrdU-positive cells significantly increased in the mucosal epithelium surrounding colonic ulcers when compared with those treated with PBS (treated with ADSCs, 28.1 ± 3.6/crypt, versus treated with PBS, 18.9 ± 4.0/crypt; $P < 0.05$; Fig. 8F).

Inoculation of ADSCs Ameliorates Colitis

Histological examination was carried out to determine whether ADSCs could reduce the inflammation induced by TNBS. Extensive ulceration with coagulative necrosis extending into the muscularis propria was observed in the untreated (PBS-injected) group, and numerous neutrophils (and relatively small numbers of mononuclear cells) were detected as inflammatory cells (Fig. 9A). In contrast with these findings, in the group injected with ADSCs, a decrease in the infiltration of inflammatory cells was clearly observed along with amelioration of edema and the concomitant enhancement of epithelial regeneration, as shown in Figure 9B. Histological score is summarized in Figure 9C.

MPO activity, an index of inflammatory response, was next determined in the colon in order to evaluate the degree of inflammation in the rats treated with ADSCs or PBS after the induction of colitis by TNBS. A significant increase in MPO activity was observed in the injured colon of colitis-model rats, and the injection of ADSCs (but not PBS) was able to reduce the local MPO activity (Fig. 9D). In addition, other inflammatory cytokines, such as TNF-α, IFN-γ, IL-1β,

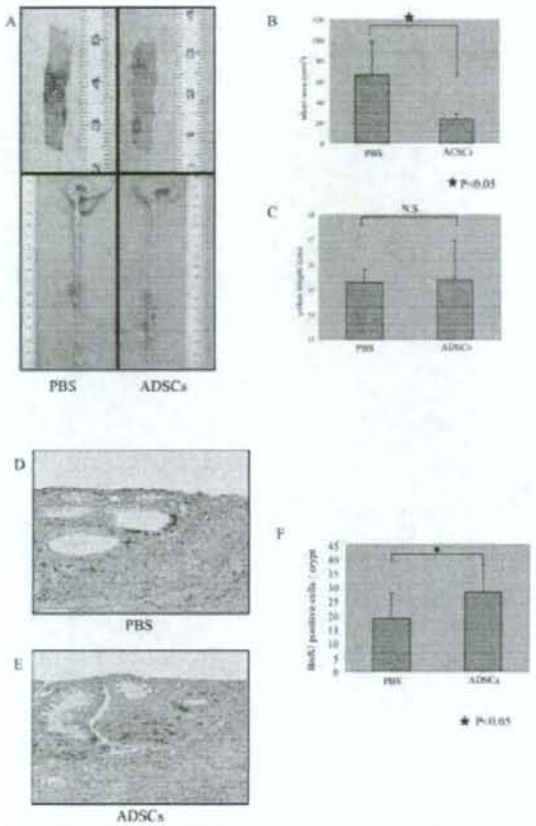

FIGURE 8. Effects of ADSCs in the repair of colonic ulcer. ADSCs or PBS submucosally injected into colitis-induced rats. A: Macroscopic examination of the area of colonic ulcers and the colon 8 days after the submucosal injection of ADSCs or PBS. B: Area of the ulcer was measured using NIH image software on pictures of the colon. C: Length (colocecal junction to anal verge) of the colon was measured by a scale. D, E: Proliferation of colonic epithelial cells was measured by injection of BrdU into rats treated with ADSCs or PBS. Representative photographs of PBS and ADSCs are shown in D and E, respectively (magnification ×400). F: BrdU-positive cells were counted, and the number of positive cells per crypt was calculated. Columns and bars represent the means ± SDs of 10 rats.

and IL-8, were examined. The expression of GRO/CINC-1 (functionally equivalent to IL-8), but not of IL-1β, TNF-α, or IFN-γ was reduced by the injection of ADSCs into the colitis-model rats (data not shown). These findings clearly show that ADSCs can ameliorate an inflammatory reaction and reduce the level of some inflammatory cytokines induced by the injection of TNBS.

Distribution and Differentiation of ADSCs In Vivo

We carried out ex vivo studies to determine whether ADSCs can differentiate into the colonic mucosa. We examined the presence of ADSCs (or ADSC-derived cells) submucosally injected by tracing Y-chromosome-positive cells with FISH (Fig. 10A–E). When compared with normal uninjured mucosal area, more than 3 times the number of ADSCs were detected in the ulcer area (22.2 ± 4.7 versus 54.4 ± 17.4 cells/field, $P < 0.05$; Fig. 10F). Most of the ADSCs were observed in the submucosal layer, whereas some were observed in the mucosal layer and in the muscularis propria. No Y-chromosome-positive cells (ADSC-derived cells) were observed in the epithelial cells, vessel component, or nerve cells (data not shown). Furthermore, Y-chromosome-positive cells were determined after staining with cytokeratin, vimentin, S-100, or SMA in order to characterize cells of ADSC origin (Fig. 11). Y-chromosome-positive cells were detected in fibroblast-like cells under the basal membrane, in smooth muscle cells in the muscle layer, and in adipose tissue. However, they were not detected in endothelial cells, the neural crest, and epithelial cells.

DISCUSSION

In the present study, we have shown that ADSCs can facilitate colonic mucosal repair and reduce the infiltration of inflammatory cells. The ADSCs used in the present study were characterized as $CD90^{+}CD45^{-}$ cells,[15,16] being similar to bone marrow–derived mesenchymal stem cells (MSCs),[1,3,4,7] and they were cytohistochemically confirmed to be functional MSCs (Figs. 4 and 5) because of their capacity to differentiate into cells with adipogenic, osteogenic, neurogenic, and epitheliogenic lineages when lineage-specific induction factors have been added to the culture, as has been previously reported.[2,9,17,18] Therefore, the ADSCs used in the present study have similar features to MSCs from the bone marrow. The proliferative capacity of the ADSCs was also similar to that of MSCs.[4,7,15,16] The doubling time of ADSCs remained unchanged until 10 passages (Fig. 3). Therefore, along with the ADSCs being easily obtained by lipoaspiration,[19] ADSCs can be a useful candidate for the source of cell therapy.

In addition, one advantage of ADSCs is their potential to secrete growth factors, such as VEGF, HGF,[20] and adiponectin,[21] which facilitate the regeneration of injured tissue alone or synergistically.[22] As has been reported, HGF regulates cell growth, motility, and morphogenesis of various types of cells, including epithelial cells and endothelial cells, and it also prevents fibrosis.[23,24] Recent studies have shown that the combination of HGF with VEGF increases neovascularization in the rat corneal assay[25] and that HGF facilitates the repair of large colonic ulcers in TNBS-induced colitis in rats.[26] Adiponectin has been reported to not only improve insulin resistance and prevent atherosclerosis, fatty liver, and

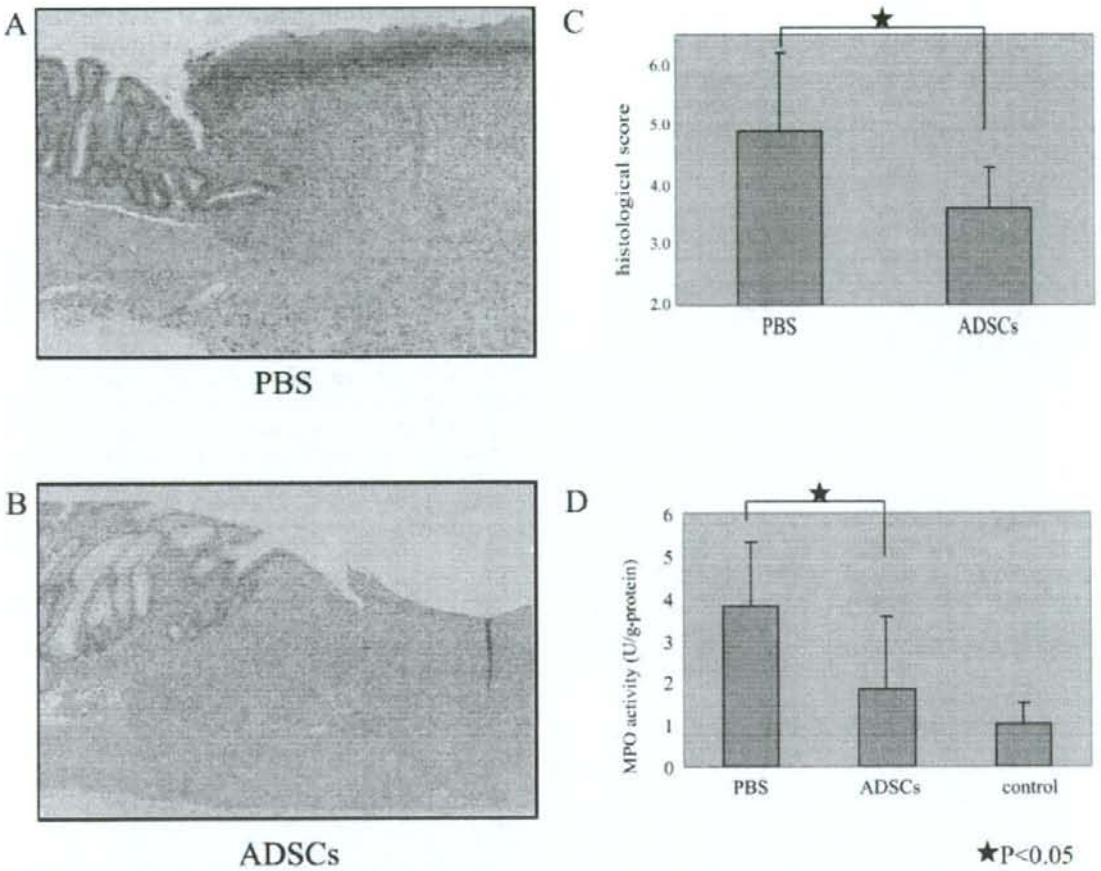

FIGURE 9. Amelioration of colitis and reduction of inflammatory responses by ADSCs. A: Histopathologic examination of colon was carried out in TNBS-induced colitis rats injected with PBS. It is noted that extensive mucosal damage and marked inflammatory cell infiltration were observed. B: Histopathologic examination of colon 8 days after injection of ADSCs; the development of regenerative epithelium, and reduced inflammatory cell infiltration and edema were observed (magnification ×100). C: Histological score of rats injected with PBS or ADSCs. D: Measurement of MPO activity. Colonic MPO activity determined 10 days after injection of PBS or ADSCs in colitis-induced rats. The rats injected with PBS alone (without injection of TNBS or ADSCs) served as controls. Columns and bars represent the means ± SDs of 10 rats ($^*P < 0.05$).

liver fibrosis but also to exert several anti-inflammatory effects.[27–30] Moreover, it has been reported that adiponectin reduces the attachment of monocytes to the endothelium by down-regulating the expression of vascular cell adhesion molecule-1, intercellular adhesion molecule-1, and E-selectin[27] and that it inhibits phagocytic activity and production of TNF-α and IL-6 from cultured macrophages.[31] These results indicate that HGF, VEGF, and adiponectin play a crucial role in intestinal mucosal wound healing. In the present study, significant amounts of HGF, VEGF, and adiponectin were detected in the culture supernatants of ADSCs (Fig. 6), indicating that ADSCs injected into the submucosa may secrete these cytokines in situ, resulting in the acceleration of regeneration of wound mucosa and also inhibition of the inflammation observed in TNBS-induced colitis. This possibility was actually confirmed by the in vivo examination in which

FIGURE 10. Distribution of ADSCs in vivo by FISH. A: Fluorescence microscopy of colon 8 days after submucosal injection of 10^7 ADSCs (×10) showing almost healed to normal mucosa. B: Ulcer area undergoing healing. C–E: Distribution of ADSCs or ADSC-derived cells (Y-chromosome-positive cells) in mucosal (C), submucosal (D), and muscular layer (E). F: Y-chromosome-positive cells were counted in 3 low-magnification fields per rat colon 8 days after submucosal injection of ADSCs. Columns and bars represent the means ± SDs of 10 rats ($^*P < 0.001$).

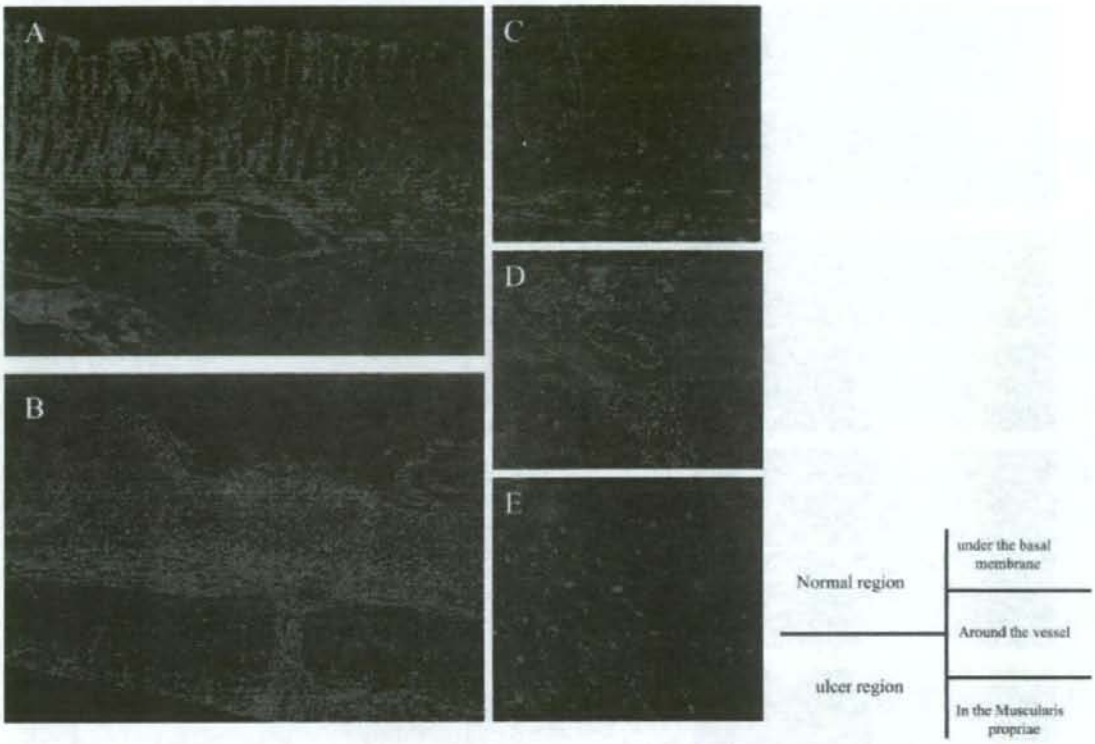
A
B
C
D
E
Normal region
ulcer region
under the basal membrane
Around the vessel
In the Muscularis propriae

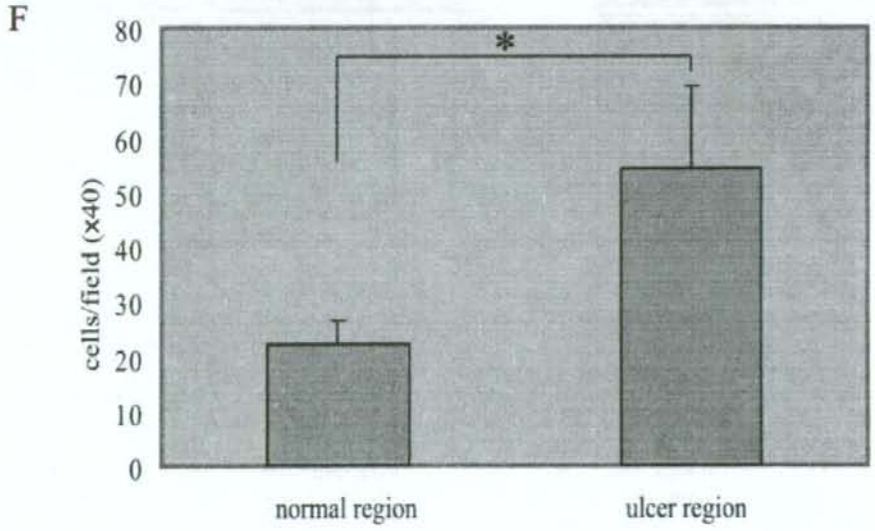
F
cells/field (x40)
80
70
60
50
40
30
20
10
0
*
normal region
ulcer region

* P<0.001

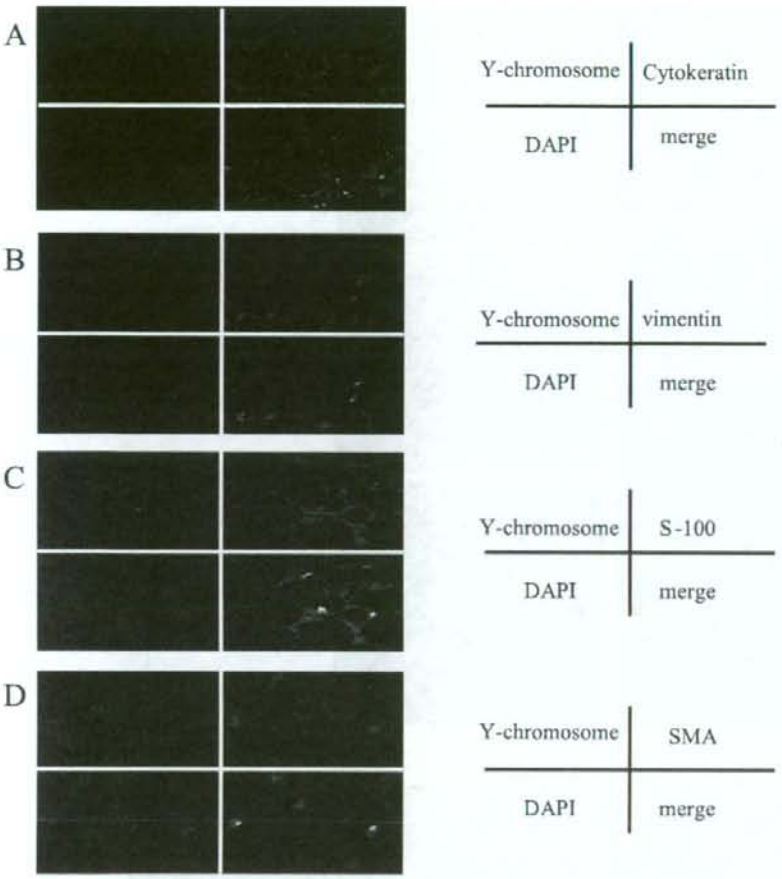

FIGURE 11. Immunofluorescent staining of Y-chromosome-positive cells. A: Y-chromosome-positive cells were not detected in epithelial cells that were stained by cytokeratin. B: Y-chromosome-positive cells were detected in fibroblast-like cells that were stained by vimentin. C: Y-chromosome-positive cells were detected in adipose tissues that were stained by S-100. D: Y-chromosome-positive cells were detected in the muscularis propria layer stained by SMA.

ADSCs facilitated the repair of colonic ulcers (Fig. 8) and reduced inflammatory responses along with TNBS-induced colitis (Fig. 9). There was no statistically significant differences in colon length between the group submucosally injected with ADSCs and the group injected with PBS. This might have been a result of the large ulcer being detected in a limited area of colon in TNBS-induced colitis-model rats in contrast to pan-colitis-model rats.

However, the decreases in the levels of IL-8 in the colonic tissue after the injection of ADSCs clearly indicate the wound-healing effects of ADSCs (Fig. 9), as also shown in the analyses of colon weight as an index of edema (Fig. 7). Furthermore, it is noted that the reduced activity of MPO observed in the colonic tissue confirms decreased infiltration of neutrophils and strengthens the effect of ADSCs. From these findings, it can be speculated that ADSCs prevent both the accumulation and the activation of neutrophils, thereby attenuating the neutrophil-dominant inflammation in colonic tissue caused by TNBS through the reduction of IL-8 levels that play a pivotal role in the accumulation of circulating leukocytes in inflammatory foci.[32] Furthermore, the effect of ADSCs might also be attributable to the anti-inflammatory effect of adiponectin, as shown in the previous study, in which adiponectin was found to exert its anti-inflammatory effect by inhibiting IL-8 production.[30] In addition, adiponectin promotes angiogenesis in response to tissue ischemia.[33] These data suggest that adiponectin secreted by ADSCs may also play a crucial role in TNBS-induced colitis.

As shown in Figure 10, cells derived from ADSCs, defined by Y-FISH, were detected in the mucosal layer under the basal membrane, the submucosal layer around the vessel, and the muscle layer; they were especially observed in the area of inflammation, such as the ulcer edge. They could be thought to differentiate into fibroblast-lineage (vimentin-positive cells), adipocyte-lineage (S-100-positive cells), and muscle-lineage cells (SMA-positive cells) when immunohis-

tochemically examined. However, they were not detected in the epithelial layer, indicating that ADSCs (submucosally injected) did not differentiate into epithelial-lineage or neural-lineage cells, even though they differentiated into various lineage cells in vitro (Figs. 4 and 5). This is in contrast with the findings that bone marrow MSCs were detected in the epithelium of the stomach and intestine[34] and differentiated into neural cells[35] and that MSCs in bone marrow seem to be more primitive than ADSCs. Therefore, our results indicate that although ADSCs have the potential to differentiate into various lineage cells in vitro, ADSCs in vivo can differentiate into mesodermal lineage cells.

Examination in vitro showed that collectively, ADSCs have multiple differentiation ability and secrete growth factors such as VEGF and HGF in large quantities and also produce adiponectin. Therefore, although we have not measured the tissue levels of these growth factors after the injection of ADSCs, it is highly feasible that ADSCs injected in vivo (1×10^7 cells) produce them and that these soluble factors might be responsible for the regeneration of the injured regions observed in the TNBS-induced colitis. Moreover, some ADSCs may differentiate into the various components of the colon, such as smooth muscles, fibroblasts, and myofibroblasts. These mesodermal cells are essential for facilitating the regeneration of epithelial cells. Furthermore, ADSCs improved TNBS-induced colitis by ameliorating colonic injury induced by proinflammatory cytokines.

Importantly, the safety of high-dose lipoaspiration to obtain ADSCs in humans was already established,[36] and thus ADSCs are a viable therapeutic option for amelioration of Crohn's disease or IBD by repairing injured intestinal mucosa. If the number of ADSCs obtained from the subcutaneous adipose tissues of the abdomens of patients themselves is enough to use for the cell therapy, ADSCs can be immediately applicable without cell culture, and the remaining ADSCs can be kept by cryopreservation for future use when a fistula recurs. In addition, treatment via endoscopy is considered a general and established method, thereby submucosally injecting ADSCs without an operation. It is feasible that in vitro cultured ADSCs inoculated into the submucosa are transformed into tumors. Therefore, we have to examine this possibility for a long life span after the treatment, and these types of experiments are now under investigation.

In conclusion, ADSCs can accelerate the regeneration of injured regions, and HGF, VEGF, and adiponectin produced by ADSCs might be responsible for the regeneration.

ACKNOWLEDGMENTS

The authors thank Mr. Hilary Eastwick-Field, Mr. Brian O'Flaherty, and Ms. K. Ando for their help in the preparation of the manuscript.

REFERENCES

1. Katz AJ, Tholpady A, Tholpady SS, et al. Cell surface and transcriptional characterization of human adipose-derived adherent stromal (hADAS) cells. *Stem Cells.* 2005;23:412–423.
2. Strem BM, Hicok KC, Zhu M, et al. Multipotential differentiation of adipose tissue-derived stem cells [review]. *Keio J Med.* 2005;54:132–141.
3. De Ugarte DA, Morizono K, Elbarbary AS, et al. Comparison of multi-lineage cells from human adipose tissue and bone marrow. *Cells Tissues Organs.* 2004;174:101–109.
4. Lee RH, Kim B, Choi I, et al. Characterization and expression analysis of mesenchymal stem cells from human bone marrow and adipose tissue. *Cell Physiol Biochem.* 2004;14:311–324.
5. Garcia-Olmo D, Garcia-Arranz M, Herreros D, et al. A phase I clinical trial of the treatment of Crohn's fistula by adipose mesenchymal stem cell transplantation. *Dis Colon Rectum.* 2005;48:1416–1423.
6. Schrepfer S, Deuse T, Reichenspurner H, et al. Stem cell transplantation: the lung barrier. *Transplant Proc.* 2007;39:573–576.
7. Kern S, Eichler H, Stoeve J, et al. Comparative analysis of mesenchymal stem cells from bone marrow, umbilical cord blood, or adipose tissue. *Stem Cells.* 2006;24:1294–1301.
8. Woodbury D, Schwarz EJ, Prockop DJ, et al. Adult rat and human bone marrow stromal cells differentiate into neurons. *J Neurosci Res.* 2000; 61:364–370.
9. Zuk PA, Zhu M, Ashjian P, et al. Human adipose tissue is a source of multipotent stem cells, *Mol Biol Cell.* 2002;13:4279–4295.
10. Brzoska M, Geiger H, Gauer S, Baer P. Epithelial differentiation of human adipose tissue-derived adult stem cells. *Biochem Biophys Res Commun.* 2005;330:142–150.
11. Morris GP, Beck PL, Herridge MS, et al. Hapten-induced model of chronic inflammation and ulceration in the rat colon. *Gastroenterology.* 1989;96:795–803.
12. Macpherson BR, Pfeiffer CJ. Experimental production of diffuse colitis in rats. *Digestion.* 1978;17:135–150.
13. Tsune I, Ikejima K, Hirose M, et al. Dietary glycine prevents chemical-induced experimental colitis in the rat. *Gastroenterology.* 2003;125: 775–785.
14. Krawisz JE, Sharon P, Stenson WF. Quantitative assay for acute intestinal inflammation based on myeloperoxidase activity. Assessment of inflammation in rat and hamster models. *Gastroenterology.* 1984;87: 1344–1350.
15. Javazon EH, Colter DC, Schwarz EJ, et al. Rat marrow stromal cells are more sensitive to plating density and expand more rapidly from single-cell-derived colonies than human marrow stromal cells. *Stem Cells.* 2001;19:219–225.
16. Yoshimura H, Muneta T, Nimura A, et al. Comparison of rat mesenchymal stem cells derived from bone marrow, synovium, periosteum, adipose tissue, and muscle. *Cell Tissue Res.* 2007;327:449–462.
17. Ashjian PH, Elbarbary AS, Edmonds B, et al. In vitro differentiation of human processed lipoaspirate cells into early neural progenitors. *Plast Reconstr Surg.* 2003;111:1922–1931.
18. Brzoska M, Geiger H, Gauer S, et al. Epithelial differentiation of human adipose tissue-derived adult stem cells. *Biochem Biophys Res Commun.* 2005;330:142–150.
19. Gimble JM, Guilak F. Adipose-derived adult stem cells: isolation, characterization, and differentiation potential. *Cytotherapy.* 2003;5:362–369.
20. Rehman J, Traktuev D, Li J, et al. Secretion of angiogenic and antiapoptotic factors by human adipose stromal cells. *Circulation.* 2004; 109:1292–1298.
21. Zvonic S, Lefevre M, Kilroy G, et al. Secretome of primary cultures of human adipose-derived stem cells: modulation of serpins by adipogenesis. *Mol Cell Proteomics.* 2007;6:18–28.
22. Van Belle E, Witzenbichler B, Chen D, Silver et al. Potentiated angiogenic effect of scatter factor/hepatocyte growth factor via induction of vascular endothelial growth factor: the case for paracrine amplification of angiogenesis. *Circulation.* 1998;97:381–390.
23. Yaekashiwa M, Nakayama S, Ohnuma K, et al. Simultaneous or delayed administration of hepatocyte growth factor equally represses the fibrotic changes in murine lung injury induced by bleomycin. A morphologic study. *Am J Respir Crit Care Med.* 1997;156:1937–1944.

24. Matsuda Y, Matsumoto K, Yamada A, et al. Preventive and therapeutic effects in rats of hepatocyte growth factor infusion on liver fibrosis/cirrhosis. *Hepatology*. 1997;26:81–89.
25. Xin X, Yang S, Ingle G, et al. Hepatocyte growth factor enhances vascular endothelial growth factor-induced angiogenesis in vitro and in vivo. Am J Pathol. 2001;158:1111–1120.
26. Numata M, Ido A, Moriuchi A, et al. Hepatocyte growth factor facilitates the repair of large colonic ulcers in 2,4,6-trinitrobenzene sulfonic acid-induced colitis in rats. *Inflamm Bowel Dis*. 2005;11:551–558.
27. Ouchi N, Kihara S, Arita Y, et al. Novel modulator for endothelial adhesion molecules: adipocyte-derived plasma protein adiponectin. *Circulation*. 1999;100:2473–2476.
28. Wulster-Radcliffe MC, Ajuwon KM, Wang J, et al. Adiponectin differentially regulates cytokines in porcine macrophages. *Biochem Biophys Res Commun*. 2004;316:924–929.
29. Wolf AM, Wolf D, Rumpold H, Enrich B, Tilg H. Adiponectin induces the anti-inflammatory cytokines IL-10 and IL-1RA in human leukocytes. *Biochem Biophys Res Commun*. 2004;323:630–635.
30. Nishihara T, Matsuda M, Araki H, et al. Effect of adiponectin on murine colitis induced by dextran sulfate sodium. *Gastroenterology*. 2006;131:853–861.
31. Yokota T, Oritani K, Takahashi I, et al. Adiponectin, a new member of the family of soluble defense collagens, negatively regulates the growth of myelomonocytic progenitors and the functions of macrophages. *Blood*. 2000;96:1723–1732.
32. Pender SL, Chance V, Whiting CV, et al. Systemic administration of the chemokine macrophage inflammatory protein 1alpha exacerbates inflammatory bowel disease in a mouse model. *Gut*. 2005;54:1114–1120.
33. Shibata R, Ouchi N, Kihara S, et al. Adiponectin stimulates angiogenesis in response to tissue ischemia through stimulation of amp-activated protein kinase signaling. *J Biol Chem*. 2004;279:28670–28674.
34. Semont A, Francois S, Mouiseddine M, et al. Mesenchymal stem cells increase self-renewal of small intestinal epithelium and accelerate structural recovery after radiation injury. *Adv Exp Med Biol*. 2006;585:19–30.
35. Sanchez-Ramos J, Song S, Cardozo-Pelaez F, et al. Adult bone marrow stromal cells differentiate into neural cells in vitro. *Exp Neurol*. 2002;164:247–256.
36. Cardenas-Camarena L. Lipoaspiration and its complications: a safe operation. *Plast Reconstr Surg*. 2003;112:1435–1441; discussion 1442–1443.

Am J Physiol Gastrointest Liver Physiol 296: G23–G35, 2009.
First published November 20, 2008; doi:10.1152/ajpgi.90225.2008.

Requirement of Notch activation during regeneration of the intestinal epithelia

Ryuichi Okamoto,[1,2] Kiichiro Tsuchiya,[2] Yasuhiro Nemoto,[2] Junko Akiyama,[2] Tetsuya Nakamura,[1,2] Takanori Kanai,[2] and Mamoru Watanabe[2]

[1]*Department of Advanced Therapeutics in Gastrointestinal Diseases and* [2]*Department of Gastroenterology and Hepatology, Graduate School, Tokyo Medical and Dental University, Tokyo, Japan*

Submitted 7 March 2008; accepted in final form 18 November 2008

Okamoto R, Tsuchiya K, Nemoto Y, Akiyama J, Nakamura T, Kanai T, Watanabe M. Requirement of Notch activation during regeneration of the intestinal epithelia. *Am J Physiol Gastrointest Liver Physiol* 296: G23–G35, 2009. First published November 20, 2008; doi:10.1152/ajpgi.90225.2008.—Notch signaling regulates cell differentiation and proliferation, contributing to the maintenance of diverse tissues including the intestinal epithelia. However, its role in tissue regeneration is less understood. Here, we show that Notch signaling is activated in a greater number of intestinal epithelial cells in the inflamed mucosa of colitis. Inhibition of Notch activation in vivo using a γ-secretase inhibitor resulted in a severe exacerbation of the colitis attributable to the loss of the regenerative response within the epithelial layer. Activation of Notch supported epithelial regeneration by suppressing goblet cell differentiation, but it also promoted cell proliferation, as shown in in vivo and in vitro studies. By utilizing tetracycline-dependent gene expression and microarray analysis, we identified a novel group of genes that are regulated downstream of Notch1 within intestinal epithelial cells, including PLA2G2A, an antimicrobial peptide secreted by Paneth cells. Finally, we show that these functions of activated Notch1 are present in the mucosa of ulcerative colitis, mediating cell proliferation, goblet cell depletion, and ectopic expression of PLA2G2A, thereby contributing to the regeneration of the damaged epithelia. This study showed the critical involvement of Notch signaling during intestinal tissue regeneration, regulating differentiation, proliferation, and antimicrobial response of the epithelial cells. Thus Notch signaling is a key intracellular molecular pathway for the proper reconstruction of the intestinal epithelia.

intestinal epithelial cells; goblet cells; PLA2G2A; ulcerative colitis

THE INTESTINAL EPITHELIA are composed of four lineages of intestinal epithelial cells (IECs) that arise from intestinal stem cells (1). Recent studies have shown that various signals such as Wnt, Sonic hedgehog, and bone morphogenetic protein interact within the stem and progenitor cells of the intestinal epithelia to finely regulate the expansion and the cell fate decision of IECs. Other studies have revealed that Notch signaling may also play critical roles in the maintenance of the intestinal epithelia (20).

Notch signaling is a signaling pathway known to regulate differentiation and proliferation of cells in diverse adult tissues (1). Activation of Notch receptor is mediated by the cleavage of its intracellular domain (NICD), and this intracellular domain translocates from the cell membrane to the nucleus, thereby functioning as a transcriptional activator of target genes such as Hes1 (10, 25). The functional role of Notch signaling in the intestine was first described in a study of Hes1-null mice; depletion of Hes1 was associated with significant increases in the secretory lineage IECs (9). Other studies have shown that the activation of Notch promoted proliferation of crypt progenitor cells and directed their cell fates toward absorptive but not secretory lineage cells (6, 28, 33). A recent study suggested that Notch might also function in postmitotic IECs, directing their cell fates toward secretory lineage cells (42). Thus these studies have suggested that Notch signaling functions in the intestine to regulate differentiation and proliferation of IECs, contributing to the maintenance and the homeostasis of the intestinal mucosa. However, the role of Notch signaling in tissue regeneration is less understood.

Damage of the intestinal epithelia is observed in a wide variety of diseases, such as acute intestinal infections, radiation injuries, or idiopathic inflammatory bowel diseases (23). Once the epithelial layer is damaged, it responds by restoring the continuity and integrated structure via activating the stepwise regeneration program (16). The initial response is called restitution, which is the redistribution of remaining IECs to rapidly cover the damaged area. This initial step is usually completed in an extremely short period of time and thus does not require the proliferation or expansion of IECs (19). However, in the next step, the rapid expansion of IECs is necessary to rebuild the proper structure of the epithelia. This response is manifested by the appearance of the regenerative epithelia in the intestine, showing a marked expansion of the proliferating compartment consisting of undifferentiated IECs. However, the exact molecular mechanisms involved in this critical step of intestinal epithelial regeneration has never been described.

Another change that is observed in the intestine during such a regenerative process is the ectopic expression of antimicrobial peptides by IECs. Paneth cells usually secrete peptides such as lysozymes, α-defensins, or PLA2G2A, and this helps to maintain the ideal environment for the stem and progenitor IECs within the small intestinal crypts. The ectopic expressions of these antimicrobial peptides by IECs are frequently observed in the inflamed colonic mucosa (5, 8), and such expressions likely support the local immune system in providing an ideal environment for the regeneration of the damaged mucosa.

In this study, we show that Notch signaling is activated in many IECs in the inflamed mucosa of murine colitis. Results show that the activation of Notch is critical for the proper regeneration program in the epithelial layer and that it helps to suppress goblet cell differentiation and promote cell proliferation. A comprehensive analysis identified a novel group of genes regulated by Notch in IECs, which included

Address for reprint requests and other correspondence: M. Watanabe, Dept. of Gastroenterology and Hepatology, Graduate School, Tokyo Medical and Dental Univ., 1-5-45 Yushima, Bunkyo-ku, Tokyo 113-8519, Japan (e-mail address: mamoru.gast@tmd.ac.jp).

The costs of publication of this article were defrayed in part by the payment of page charges. The article must therefore be hereby marked "*advertisement*" in accordance with 18 U.S.C. Section 1734 solely to indicate this fact.

a gene encoding an antimicrobial peptide called PLA2G2A. Such functions of Notch activation were present not only in the mice intestine but also in the human intestine. Finally, the clinical relevance of Notch-mediated regeneration is analyzed in ulcerative colitis (UC). Thus Notch signaling is a key-signaling pathway involved in intestinal tissue regeneration, in fine regulation of differentiation and proliferation, and in antimicrobial activities in IECs. Our findings point to a novel molecular target for agents that could promptly regenerate the intestinal mucosa in a wide range of intestinal diseases.

MATERIALS AND METHODS

Mice. C57BL/6J mice at 8 wk of age were purchased from Japan Clea. Mice were housed and maintained in the animal facility of Tokyo Medical and Dental University. The institutional animal use and care committee approved the study.

In vivo experiments. Induction of colitis was performed as previously described (17). Briefly, mice were fed ad libitum with 1.75% dextran sodium sulfate (DSS, Bio Research of Yokohama) for 5 consecutive days, followed by distilled water for another 5 days. For inhibition of Notch activation, mice were orally administered with either 5% DMSO (vehicle, VEC) or LY411,575 (LY) (10 mg/kg) dissolved in 0.5% (wt/vol) methylcellulose (WAKO), once daily for 5 consecutive days. Twenty-four mice were separated into four groups: *1*) fed distilled water for five days followed by daily administration of vehicle alone (VEC, $n = 6$) for 5 days, *2*) fed distilled water for 5 days followed by daily administration of LY411,575 (LY, $n = 6$) for five days, *3*) fed 1.75% DSS for 5 days followed by daily administration of vehicle (DSS + VEC, $n = 6$) for 5 days, and *4*) fed 1.75% DSS for 5 days followed by daily administration of LY411,575 (DSS + LY, $n = 6$) for 5 days. The whole body weights of mice were measured everyday. They were euthanized 12 h after the final administration. Colonic tissues were subjected to hematoxylin and eosin staining and analyzed by histological scoring following the criteria described elsewhere (21). Flow cytometry of thymocytes and splenocytes were performed as previously described (35, 41).

Immunoblot analysis. Immunoblots were performed as described elsewhere (18). The primary antibodies used were anti-Cleaved Notch1 (1:1,000, Cell Signaling Technology), anti-Hes1 (1:4,000, a kind gift from Dr. T. Sudo), and anti-β-actin (1:5,000, Sigma). Proteins were visualized either by the ECL Advance Western Blotting Kit (GE Healthcare) or ECL Western Blotting Kit (GE Healthcare).

Cell culture. The cell cultures and transfections of plasmid DNA were performed as described elsewhere (18). The inhibition of Notch signaling was achieved by the addition of LY411,575 (1 μM), synthesized according to Wu et al. (38). A cell line expressing Notch1 intracellular domain (Tet-On NICD1 cells) under the control of tetracycline or doxycycline (DOX, 100 ng/ml, Clontech) was generated as described elsewhere (18), using LS174T cells as parent cells. The cell lines were supplemented with Blasticidin (7.5 μg/ml, Invitrogen) and Zeocin (750 μg/ml, Invitrogen) for their maintenance.

RT-PCR assays. RT-PCR was performed as described elsewhere (18). Quantitative analyses using the SYBR green master mix (Qiagen) was performed by ABI 7500 (Applied Biosystems). Primer sequences for human β-actin, G3PDH, or MUC2 have been previously described (30). The primer sequences for other genes are summarized in Table 1. The results are shown as the means of the data collected from two rounds of assays, with each assay performed in triplicate. The data were statistically analyzed with paired Student's *t*-tests.

Human intestinal tissue specimens. Human tissue specimens were obtained from patients who underwent surgery for the treatment of Crohn's disease, UC, or colon cancer at Yokohama Municipal General Hospital or Tokyo Medical and Dental University Hospital. Written informed consent was obtained from each patient, and the study was approved by the ethics committee of Yokohama Municipal General Hospital and Tokyo Medical and Dental University.

Immunohistochemistry. Immunohistochemistry using intestinal tissues has been described elsewhere (12). The same antibodies used in immunoblot analysis were also used for the immunohistological staining of NICD1 and Hes1. The other antibodies used were anti-human Ki-67 (1:50, MIB-1, DAKO), anti-human PLA2G2A (1:200, sc-14468, Santa Cruz Biotechnology), anti-human MUC2 (1:100, Ccp58, Santa Cruz Biotechnology), and anti-mouse Ki-67 (1:50, TEC-3, DAKO). Microwave treatment (500 W, 10 min) in 10 mM citrate buffer was required for staining human tissues in Hes1, Ki-67, and NICD1 and for staining mice tissues in Ki-67. The tyramide signal amplification (Molecular Probes) was used for immunofluorescent detection of NICD1. Staining was visualized by an avidin-biotin-peroxidase complex (ABC) elite kit (Vector) using diaminobenzidine as a substrate or by secondary antibodies conjugated with Alexa-594 or Alexa-488 (Molecular Probes). The quantification of Hes1 (Fig. 1*B*), Alcian blue, Ki-67, or NICD1 (Fig. 8*B*) was conducted by the examination of nine randomly selected longitudinal sections of crypts selected from at least three different individuals. The data were statistically analyzed with paired Student's *t*-tests.

Microarray. Microarray analysis was performed using the Acegene human oligo chip 30K subset A (Hitachi software). Total RNA was collected before and after 24 h of NICD1 expression in LS174T cells and labeled using the Amino Aryll Message Amp aRNA kit (Ambion). The complete dataset of the analysis has been submitted to the NCBI Gene Expression Omnibus (GEO) and is accessible through GEO accession number GSE10136.

Table 1. *Primers used in the present study*

Gene	Primer Sequence	
	Forward	Reverse
Human Hes1	5′- ATGCCAGCTGATATAATGGAG -3′	5′- TCACCTCGTTCATGCACTCG -3′
Human Notch1	5′- CCGAACCAATACAACCCTCT -3′	5′- GCGATCTGGGACTGCTGCATGCT -3′
Human PLA2G2A	5′- ACCATGAAGACCCTCCTACTG -3′	5′- GAAGAGGGGACTCAGCAACG -3′
Mouse Hes1	5′- TCAACACGACACCGGACAAACC -3′	5′- GGTACTTCCCCAACACGCTCG -3′
Mouse MUC2	5′- TCCACCATGGGGCTGCCACT -3′	5′- GGCCCGAGAGTAGACCTTGG -3′
Mouse TNF-α	5′- CTACTGGCGCTGCCAAGGCTGT -3′	5′- GCCATGAGGTCCACCACCCTG -3′
Mouse IFN-γ	5′- ACACTGCATCTTGGCTTTGC -3′	5′- CGGATGAGCTCATTGAATGCT -3′
MouseIL-1α	5′- CCCGTCCTTAAAGCTGTCTG -3′	5′- AATTGGAATCCAGGGGAAAC -3′
Mouse IL-1β	5′- TTGACGGACCCCAAAAGAT -3′	5′- GAAGCTGGATGCTCTCATCTG -3′
Mouse IL-6	5′- GCTACCAAACTGGATATAATCAGGA -3′	5′- CCAGGTAGCTATGGTACTCCAGAA -3′
Mouse PLA2G2A	5′- AAGAAGCCCAAATGCTGAAA -3′	5′- TTTATCACCGGGAAACTTGG -3′
Mouse β-actin	5′- CCTAAGGCCAACCGTGAAAAG -3′	5′- TCTTCATGGTGCTAGGAGCCA -3′

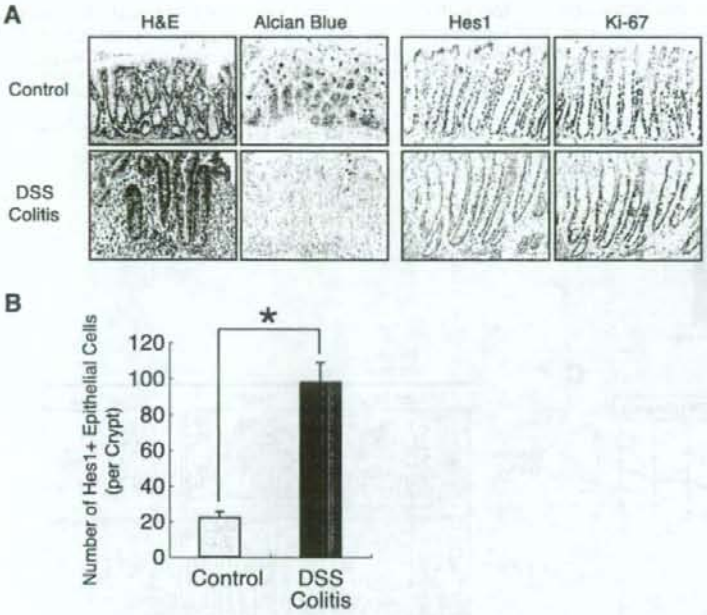

Fig. 1. Activation of Notch signaling is increased in crypts of dextran sodium sulfate (DSS)-induced colitis. *A*: histological analysis of DSS-induced colitis showing a decrease in mucin-producing intestinal epithelial cells (IECs) and an increase in Hes1- and Ki-67-expressing IECs within the crypts of the colitic mucosa. Blue staining with Alcian blue represents mucin production, whereas brown staining with diaminobenzidine (DAB) shows positive staining for Hes1 or Ki-67 (original magnification ×400). *B*: quantitative analysis of Hes1-positive IECs in crypts of normal or colitic mucosa. Data are shown as number of Hes1-positive cells per crypt on the basis of the analysis of immunohistochemical stainings. Error bars represent SD. $*P < 0.05$ on the Student's *t*-test. H & E, hematoxylin and eosin.

Plasmids. Hes1p-Luc, containing six tandem-repeats of the RBP-Jk binding site, was a kind gift from Dr. Kageyama (Kyoto, Japan). PLA2-Luc was generated by cloning a 2778-bp sequence 5′ of the human PLA2G2A gene (corresponding to −2,758 to + 20 of the promoter region) into a pGL3 basic vector (Promega). MUC2-Luc (40) was a kind gift from Dr. Yuasa (Tokyo, Japan). Tetracycline-dependent expression of NICD1 was achieved by cloning the gene encoding the intracellular portion of the mouse Notch1 (amino acid 1,704-2,531) into the pcDNA4/TO/myc-his vector (Invitrogen). All constructs were confirmed by DNA sequencing.

Immunostaining of cultured cells. Staining of cultured cells has been previously described (30). Detection of the MUC2 antibody was carried out either by the standard ABC method or by the Alexa 594-conjugated secondary antibody (Molecular Probes). The quantification of cells positive for MUC2 staining was performed by examining six randomly selected fields (three fields each in two individual counts) under ×400 magnification. The data were statistically analyzed with paired Student's *t*-tests.

ELISA. For PLA2G2A protein quantification, 1×10^6 cells were cultured in 2 ml of medium with or without DOX and analyzed with the human-PLA2 enzyme immunoassay kit (Cayman Chemicals). The incorporation of BrdU was examined by seeding cells at various cell densities in the 96-well plate, supplemented with DMSO or LY411,575. The BrdU was added 8 h before the end of culture, and the cells were subjected to analysis with the cell proliferation ELISA kit (Roche Diagnostics). The results are shown as the means of data collected by two rounds of assays, with each assay performed in triplicate. The data were statistically analyzed with paired Student's *t*-tests.

Reporter assays. The reporter assay was performed as previously described (18). Each assay was performed in triplicate, and the results were normalized using the *Renilla* luciferase activity. The results are shown as the means of normalized arbitrary units, and the data were statistically analyzed with paired Student's *t*-tests.

RESULTS

Hes1 is expressed in crypt epithelial cells of DSS-colitis. Since previous studies have evaluated the contribution of Notch signaling in the maintenance of mice intestinal epithelium (28, 33, 34), we sought to examine the role of Notch signaling in mice colitis. At first, we analyzed the expression of Hes1, a direct target gene of Notch, in mice with colitis induced by the oral administration of DSS (DSS-colitis, Fig. 1*A*). In the normal colon, crypts are predominantly composed of mature goblet cells that produce mucin. In such crypts, Hes1 is expressed in IECs residing at the lowest part of the crypt, which is also where Ki-67-positive IECs are found. In sharp contrast, the clear loss of mucin production was observed in the inflamed mucosa of DSS-colitis mice. The expressions of both Hes1 and Ki-67 were observed in a larger population of IECs, which were distributed from the bottom to the most upper regions of the crypt, suggesting that Notch signaling was activated in these IECs. The quantitative analysis of the immunostaining revealed significant increases in Hes1-positive IECs within the crypts of the DSS-colitis mice (Fig. 1*B*). These findings suggested that Notch signaling is activated in a greater number of IECs in DSS-colitis, which might be closely related with the greater number of proliferating IECs and the loss of mucin-producing IECs.

LY411,575 inhibits Notch activation and promotes goblet cell differentiation in mice intestine. To further examine the role of Notch signaling in colitis, we used LY411,575, a γ-secretase inhibitor (GSI) that is known to block Notch activation in vivo (14, 27, 36). Oral administration of LY411,575 for 5 consecutive days significantly reduced the expression of

Hes1 mRNA in mice intestine, suggesting that Notch activation was inhibited (Fig. 2*A*). In contrast, the expression of MUC2 mRNA was significantly increased by LY411,575, suggesting that the number of goblet cells increased. Consistent with this, histological analysis showed marked increases in mucus-producing IECs in the intestines of the LY411,575-treated mice (Fig. 2*C*). Consistent with reports from previous studies (27, 36), these results showed that LY411,575 could

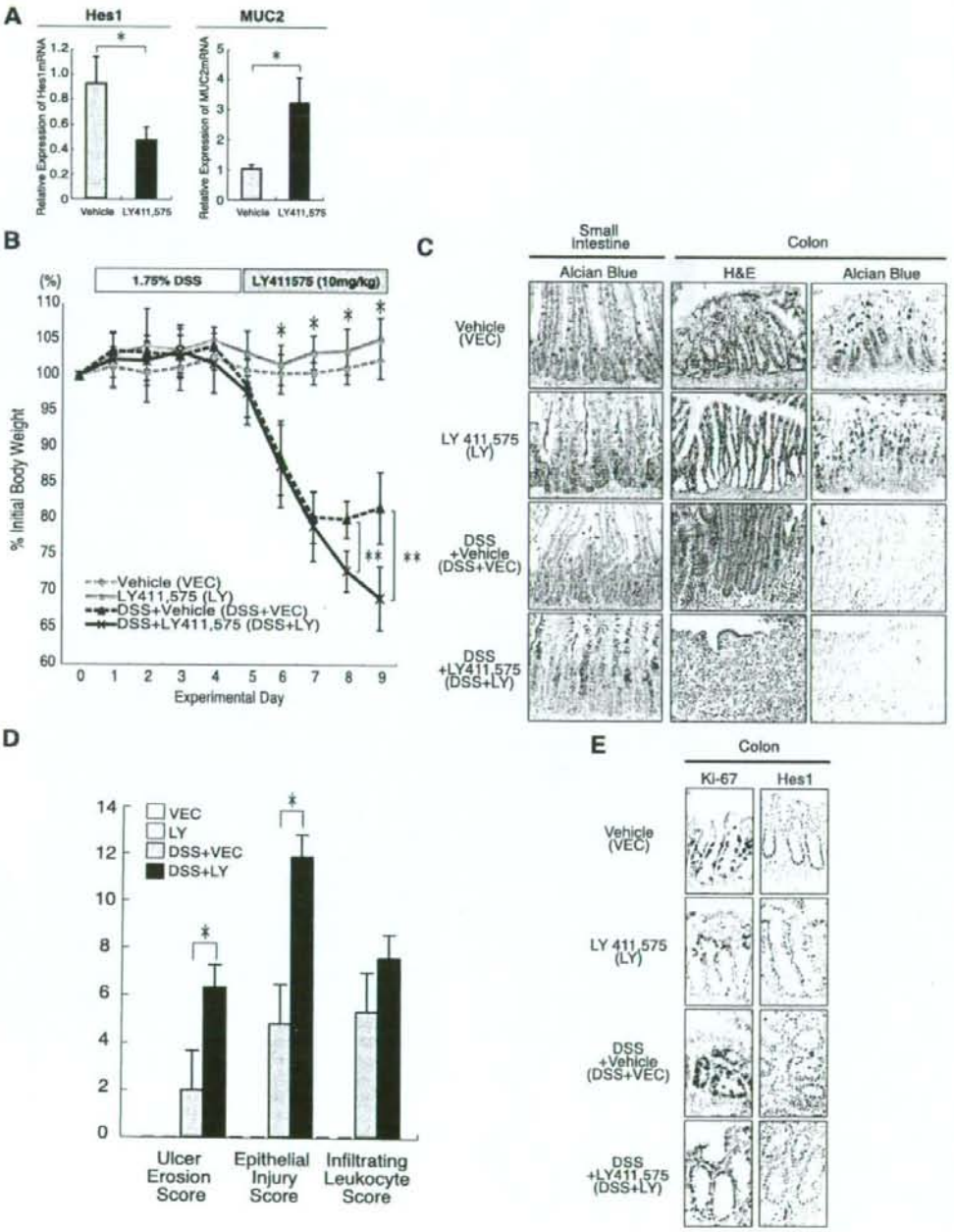

simultaneously inhibit Notch activation and promote differentiation to goblet cells in the mice intestine.

We also found marked atrophy of the thymus in LY411,575-treated mice (Supplemental Fig. S1*A*). Supplemental data for this article are available on the *American Journal of Physiology Gastrointestinal and Liver Physiology* website. Further analysis of the thymus revealed that the total number of thymocytes was significantly reduced (Supplemental Fig. S1*B*) and that the tissue architecture was disrupted (Supplemental Fig. S1*C*). Analysis of CD4/CD8 expression revealed a significant proportional reduction in double-positive cells (Supplemental Fig. S1*D*) and a reduction in the absolute number of cells (Supplemental Fig. S1*E*), suggesting that there was a significant loss of immature cells in the thymus with LY411,575 treatment. However, such an effect of LY411,575 was not present in the spleen (Supplemental Fig. S1, *A–E*). These findings clearly showed that the LY411,575 treatment had a systemic effect, affecting the thymus in addition to the intestine.

LY411,575 exacerbates DSS-colitis by impairing epithelial regeneration. Using the methods described, we designed an experiment to examine the effect of Notch inhibition during colitis (Fig. 2*B*). Mice were separated into four groups: vehicle alone (VEC), LY411,575 alone (LY), DSS with vehicle (DSS + VEC), and DSS with LY411,575 (DSS + LY). As of *day 5*, the total body weights showed significant reductions from *day 0* in DSS-treated mice (Fig. 2*B*) compared with the weights of those without DSS (the day when DSS treatment was started is designated as *day 0*). However, the DSS + LY mice showed even greater reductions in weight as of *day 8*; their reductions in body weight were significantly greater than the weight reductions in DSS + VEC mice (Fig. 2*B*). This severe loss of body weight observed in DSS + LY mice was also fatal because two mice in this group were dead at the time of euthanasia (fatality rate = 2/6, 33.3%). No deaths were observed in any other experimental group. These results suggested that LY411,575 significantly exacerbates the clinical course of DSS-colitis. A histological analysis of LY or DSS + LY mice showed a marked increase in goblet cells in the small intestine, confirming the effect of LY411,575 treatment (Fig. 2*C*). The increase in goblet cells was also observed in the colon of LY mice. A histological analysis of DSS + VEC mice showed a clear induction of colitis, as shown by the marked increase in inflammatory cells and the elongation of goblet cell depleted crypts. However, in sharp contrast, DSS + LY mice showed a severe loss of the epithelial layer in addition to an infiltration of inflammatory cells, which appeared to lack signs of epithelial regeneration (Fig. 2*C*). A histological scoring of the colonic tissues revealed increased ulcer formation and epithelial injury in DSS + LY mice compared with DSS + VEC mice, whereas no significant changes were observed in the degree of inflammation (Fig. 2*D*). Consistent with this, the mRNA expression of proinflammatory cytokines was increased in the colon of DSS-treated mice, but no clear differences were observed between DSS + VEC and DSS + LY mice (Supplemental Fig. S2).

For further analysis, we examined the expression of Hes1 and Ki-67 in the inflamed region of the colonic tissues. An increase in Hes1- or Ki-67-positive IECs was confirmed in DSS + VEC mice (Fig. 2*E*). However, both Hes1 and Ki-67 expression appeared to be markedly lost in the colonic crypts upon LY411,575 treatment (Fig. 2*E*). These results indicated that LY411,575 inhibits Notch activation and promotes goblet cell differentiation but also strongly inhibits proliferation of IECs, leading to a poor regenerative response and a severe exacerbation of DSS-colitis.

LY411,575 promotes goblet cell differentiation but inhibits proliferation of IECs in vitro. Previous in vivo results suggested that Notch activation might play critical roles in both the differentiation and proliferation of IECs. We further examined the in vitro effect of LY411,575 upon human colonic epithelial cell lines LS174T and HT29. As shown by the immunoblot analysis, the endogenous expression of both NICD1 and Hes1 was completely inhibited within LS174T cells by LY411,575 treatment (Fig. 3*A*). Consistent with this, RT-PCR analysis showed a marked decrease in Hes1 mRNA expression with LY411,575, which was maintained for up to 72 h (Fig. 3*B*). These data confirmed that LY411,575 could directly inhibit the activation of Notch within IECs.

Under this condition, we examined whether LY411,575 could promote goblet cell differentiation in vitro. Quantitative RT-PCR analysis showed a significant increase in MUC2 mRNA expression with LY411,575 treatment in both LS174T and HT29 cells (Fig. 3*C*). Consistent with this, a marked induction of MUC2 protein expression was observed in both of the cell lines that were treated with LY411,575 (Fig. 3*D*, red signal), resulting in a significant increase in the MUC2-positive cell population (Fig. 3*E*). The Alcian blue staining also showed a marked increase in mucin-producing cells in both cell lines with LY411,575 (Fig. 3*F*, black arrow). However, LY411,575 appeared to inhibit the proliferation of both cell lines since the incorporation of BrdU was significantly downregulated by LY411,575 (Fig. 3*G*). These results collectively showed that LY411,575 could directly inhibit Notch activation in IECs, which might subsequently promote goblet cell differentiation but also inhibit cell proliferation.

Activation of Notch1 suppresses goblet cell phenotype, but upregulates PLA2G2A secretion in human IECs. To further analyze the function of Notch activation in IECs, we gen-

Fig. 2. Inhibition of Notch activation by LY411,575 exacerbates DSS-colitis by impairing epithelial regeneration. *A*: LY411,575 suppresses Hes1 expression but also promotes MUC2 expression in mice intestine. After oral administration of LY411,575 or vehicle alone for 5 consecutive days, the small intestinal tissues of mice were subjected to quantitative RT-PCR analysis. Results from 3 mice in each group. Error bars represent SD. $*P < 0.05$ on the Student's *t*-test. *B*: LY411,575 significantly exacerbated wasting disease caused by DSS. As described in MATERIALS AND METHODS, mice were separated into 4 groups, and the body weight of each mouse was monitored throughout the experimental period. Error bars represent SD. $*P < 0.05$ for the difference between mice that were DSS treated (DSS + VEC and DSS + LY) or not treated (VEC and LY). $**P < 0.05$ for the difference between DSS + VEC and DSS + LY mice on the Student's *t*-test. *C*: LY411,575 exacerbated epithelial injury of DSS-colitis. Intestinal tissues of mice shown in *B* were subjected to histological analysis. Blue staining with Alcian blue represents mucin production (original magnification ×400). *D*: LY411,575 had no significant effect on inflammation of DSS-colitis. Histological scoring of colonic tissues obtained from each mice group is shown. Error bars represent SD. $*P < 0.05$ on the Student's *t*-test. *E*: LY411,575 inhibited proliferation of IECs via downregulation of Notch activity. Colonic tissues of mice were subjected to immunohistochemical staining for Hes1 and Ki-67. A less inflamed region was chosen for analysis of DSS + LY mice because the most inflamed region showed complete loss of the epithelial layer. Note that IECs expressing Hes1 or Ki-67 were confined within a narrow region of the colonic crypt in mice treated with LY411,575 (LY and DSS + LY).

erated a subline of LS174T cells (Tet-On NICD1 cells), in which forced expression of NICD1 could be induced in a tetracycline- or DOX-dependent manner. Immunoblot analysis of Tet-On NICD1 cells showed a clear induction of NICD1 and a subsequent increase in Hes1, with DOX addition (Fig. 4*A*). Consistent with this, the reporter activity of Hes1p-Luc was significantly upregulated with the induction of NICD1 in Tet-On NICD1 cells, indicating that there was an upregulation of the transcriptional activity of the Hes1 gene (Fig. 4*B*). These results confirmed that Tet-On NICD1 cells could express the functional NICD1 protein with DOX addition.

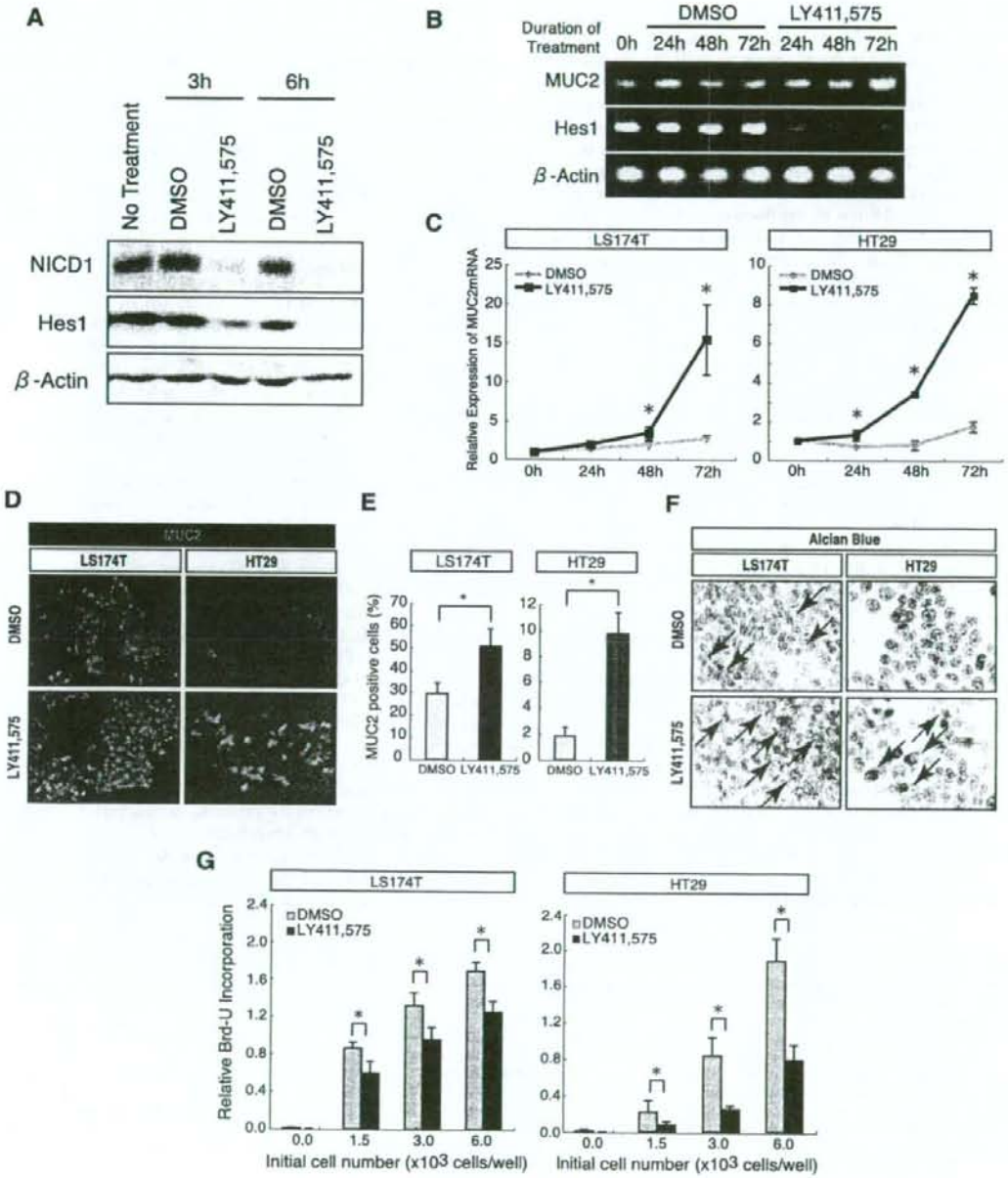

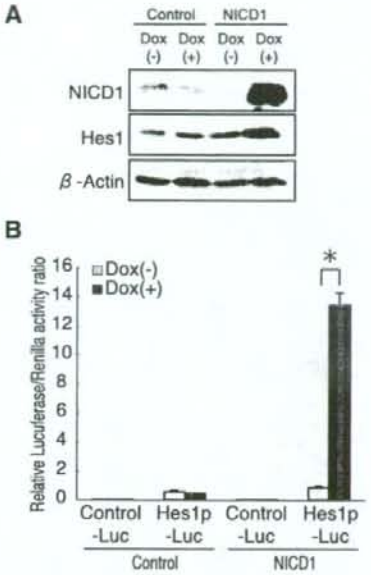

Fig. 4. Activation of Notch1 upregulates Hes1 expression in human IECs. *A*: establishment of a subline of LS174T cells expressing NICD1 under control of a tetracycline-dependent promoter (Tet-On NICD1 cells, designated as NICD1). Immunoblot analysis of Tet-On NICD1 cells showed a clear upregulation of both NICD1 and Hes1 expression with doxycycline (DOX) addition, whereas parental cells (designated as Control) remain unchanged. A low-sensitivity substrate (ECL) was used for visualization. *B*: transcriptional activity of Hes1 was upregulated with the expression of NICD1. Transcriptional activities of Hes1 gene in Tet-On NICD1 cells or control cells were analyzed by luciferase reporter assays using Hes1p-Luc. A reporter plasmid containing only the core-promoter of chicken β-actin gene served as a control (Control-Luc). Luciferase activities were measured after 12 h of culture with or without DOX. Error bars represent SD. $*P < 0.05$ on the Student's *t*-test.

Using this cell line, we found that the upregulation of NICD1 expression in LS174T cells significantly downregulated MUC2 mRNA expression (Fig. 5*A*). Further analysis with a microarray identified a group of genes that were up- or downregulated with NICD1 expression (Supplemental Tables 1 and 2). Among these genes, we focused on PLA2G2A, a gene expressed by Paneth cells, as it showed the most significant induction with NICD1 expression. Quantitative RT-PCR confirmed an upregulation of PLA2G2A mRNA expression with the NICD1 expression (Fig. 5*A*). Consistent with this, although the MUC2 protein expression was markedly suppressed (Fig. 5*B*), with resulting significant decreases in MUC2-positive cells (Fig. 5*C*) and mucin-producing cells (Fig. 5*D*), the PLA2G2A secretion was upregulated with NICD1 expression (Fig. 5*E*). These changes appeared to be regulated at the transcriptional level since the reporter activities of MUC2-Luc and PLA2-Luc showed a significant decrease and increase, respectively, with NICD1 expression (Fig. 5*F*). These results showed that, although the activation of Notch1 within LS174T cells suppressed goblet cell phenotype, it also upregulated the secretion of PLA2G2A, suggesting that the activation of Notch1 might surprisingly promote the acquisition of the specific functions of Paneth cells.

Notch1 is activated in crypt epithelial cells of the human intestine. Since we found that Notch signaling might regulate cell proliferation, goblet cell differentiation, and Paneth cell-specific function within IECs, we sought to clarify its relevance in human intestinal diseases. We first examined whether components of the Notch signaling pathway are expressed in the human intestine. An RT-PCR analysis of human intestinal tissues or epithelial cell lines successfully detected mRNAs of both Notch1 and Hes1 (Fig. 6*A*). The immunohistochemistry for NICD1 and Hes1 revealed that these proteins are expressed in the nuclei of crypt IECs (Fig. 6*B*). Similar to our observations in mice, the distribution of NICD1-positive or Hes1-positive IECs corresponded to that of Ki-67-positive IECs (Fig. 6*B*). Also, a magnified view of the staining showed a positive staining of NICD1 in columnar-shaped IECs and Paneth cells (Fig. 6*B*, black arrow) but not in goblet-shaped IECs (Fig. 6*B*, red arrowhead). Double staining of MUC2 and NICD1 confirmed the lack of NICD1 expression in goblet cells (Fig. 7*A*), whereas double staining of PLA2G2A and NICD1 confirmed expression of NICD1 in Paneth cells (Fig. 7B). These results strongly suggested that the NICD1 might function in vivo in the human intestine in a similar manner as was revealed in the in vitro study.

Increased activation of Notch1 is observed in the mucosa of UC. UC is one of the major forms of inflammatory bowel diseases, characterized by the persistent inflammation and ulcer formation in the colon. In the active region of UC, a loss of goblet cells, an ectopic expression of Paneth cell genes, and an increase in IEC proliferation are all known to be common pathological findings (7, 8, 13, 23). Thus our results strongly suggested that all of these pathological findings in UC might be mediated by the activation of Notch1 in IECs. We performed

Fig. 3. Inhibition of Notch activation promotes differentiation of goblet cells but suppresses proliferation of human IECs. *A*: LY411,575 downregulated expression of Notch1 intracellular domain (NICD1) and Hes1 in LS174T cells. Immunoblot analysis of LS174T cells treated with LY411,575 showing downregulation of endogenous NICD1 and Hes1 expression within 6 h from treatment. Cells treated with DMSO alone served as control. A high-sensitivity substrate (ECL Advance) was used for visualization. *B*: LY411,575 upregulated expression of MUC2 in LS174T cells. LS174T cells were subjected to semiquantitative RT-PCR analysis after treatment with either LY411,575 or DMSO. Note that expression of Hes1 was markedly decreased, whereas expression of MUC2 was increased after 72 h of treatment with LY411,575. *C*: LY411,575 significantly increased expression of MUC2 mRNA in both LS174T and HT29 cells. Cells were subjected to quantitative RT-PCR analysis after 0, 24, 48, and 72 h of treatment with either LY411,575 or DMSO. Error bars represent SD. $*P < 0.05$ for the difference between DMSO and LY411,575 treatment at the same time points on the Student's *t*-test. *D*: LY411,575 induced expression of MUC2 protein (red) in LS174T and HT29 cells. Cells were subjected to immunofluorescent staining of MUC2 after 72 h of treatment with either LY411,575 or DMSO (original magnification ×200). *E*: LY411,575 significantly increased the MUC2-positive cell populations among LS174T and HT29 cells. Quantitative analysis of *D* is shown by percent of MUC2-positive cells within total nucleated cells. Error bars represent SD. $*P < 0.05$, on the Student's *t*-test. *F*: LY411,575 induced mucin production in LS174T and HT29 cells. Cells were subjected to Alcian blue staining (black arrow) after 72 h of treatment with either LY411,575 or DMSO (original magnification ×400). *G*: LY411,575 significantly downregulated proliferation of LS174T and HT29 cells. A significant decrease in BrdU incorporation was observed with LY411,575 treatment in LS174T and HT29 cells. Incorporation of BrdU was measured by ELISA. Results are shown as arbitrary units of relative BrdU incorporation. Error bars represent SD. $*P < 0.05$ on the Student's *t*-test.

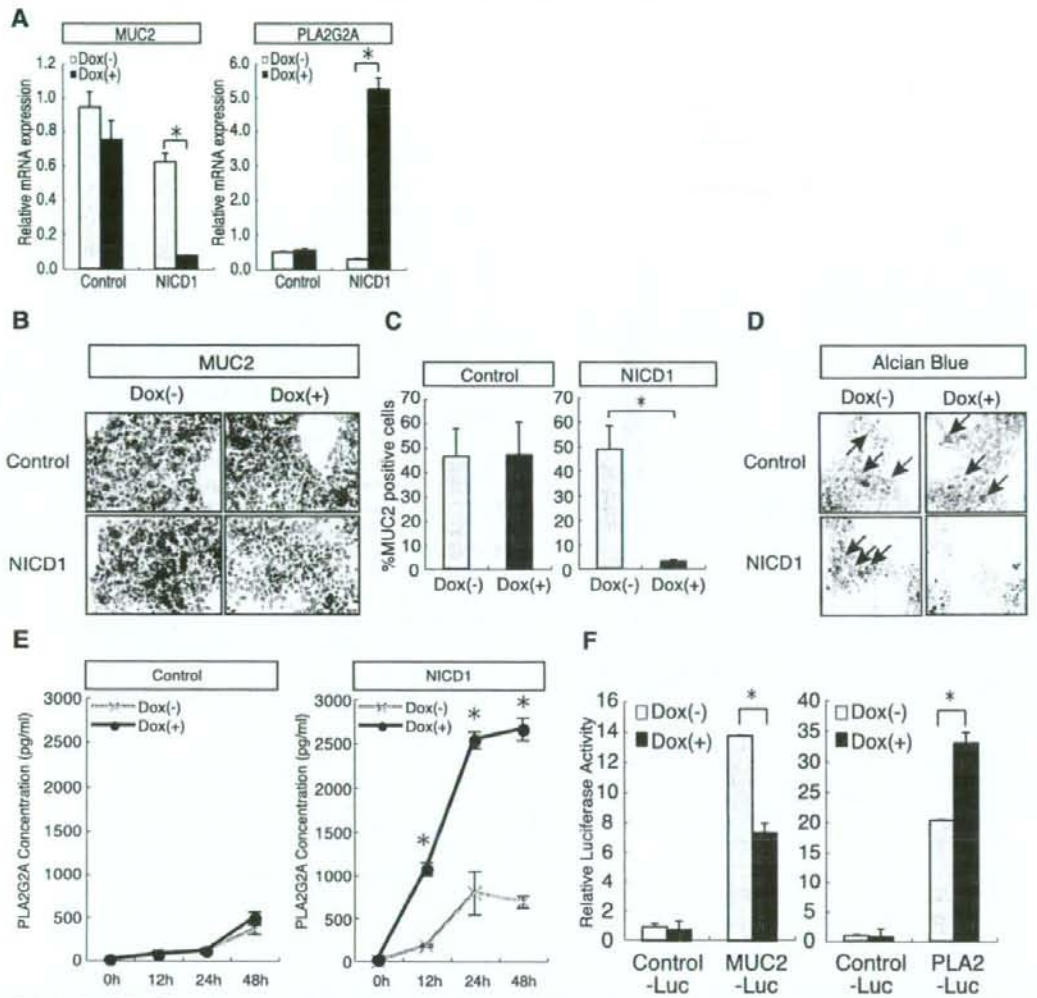

Fig. 5. Activation of Notch1 suppresses goblet cell differentiation but promotes expression of PLA2G2A of human IECs. *A*: expression of NICD1 in LS174T cells downregulated the expression of MUC2 but upregulated the expression of PLA2G2A. Quantitative RT-PCR analysis of MUC2 and PLA2G2A expression in Tet-On NICD1 cells and control cells is shown. Cells were subjected to analysis after 48 h of culture with or without DOX. Error bars represent SD. $*P < 0.05$ on the Student's *t*-test. *B*: expression of NICD1 in LS174T cells downregulated MUC2 protein expression. Tet-On NICD1 cells or control cells were subjected to immunostaining of MUC2 after 48 h of culture with or without DOX. Brown staining with DAB showed positive staining for MUC2 (original magnification ×200). *C*: expression of NICD1 in LS174T cells significantly reduced the number of cells expressing MUC2. Quantitative analysis of immunostaining shown in *B* is shown. Number of cells positively stained for MUC2 was counted and shown as percent of total nucleated cells. Error bars represent SD. $*P < 0.05$ on the Student's *t*-test. *D*: expression of NICD1 suppressed mucin production by LS174T cells. Tet-On NICD1 cells or control cells were treated as described in *B* and subjected to Alcian blue staining. The blue staining represents mucin-producing cells. (black arrow, original magnification ×800). *E*: expression of NICD1 upregulated PLA2G2A secretion of LS174T cells. Tet-On NICD1 cells or control cells were cultured with or without DOX, and culture supernatants collected at various time points were subjected to quantification of PLA2G2A using ELISA. Error bars represent SD. $*P < 0.05$ compared between DOX (+) and DOX (-) on the Student's *t*-test. *F*: expression of NICD1 in LS174T cells downregulated transcriptional activity of MUC2 gene but upregulated transcriptional activity of PLA2G2A gene. Transcriptional activity of MUC2 gene and PLA2G2A gene were measured by luciferase reporter assays using MUC2-Luc and PLA2-Luc as a reporter plasmid, respectively. pGL3-basic served as a control (Control-Luc). Luciferase activities in Tet-On NICD1 cells were analyzed after 12 h of culture with or without DOX. Error bars represent SD. $*P < 0.05$ on the Student's *t*-test.

histological analysis and found that in the crypts of UC, mucin production is markedly decreased (Fig. 8*A*, *top*, blue), whereas the number of Ki-67-expressing cells are markedly increased, distributing from the bottom to the uppermost part of the crypt (Fig. 8*A*, *bottom*, brown). In such crypts, NICD1-expressing cells showed the same distribution as Ki-67-expressing cells (Fig. 8*A*, *middle*, brown), suggesting that Notch1 is activated in an expanded proliferating cell population within the crypts of

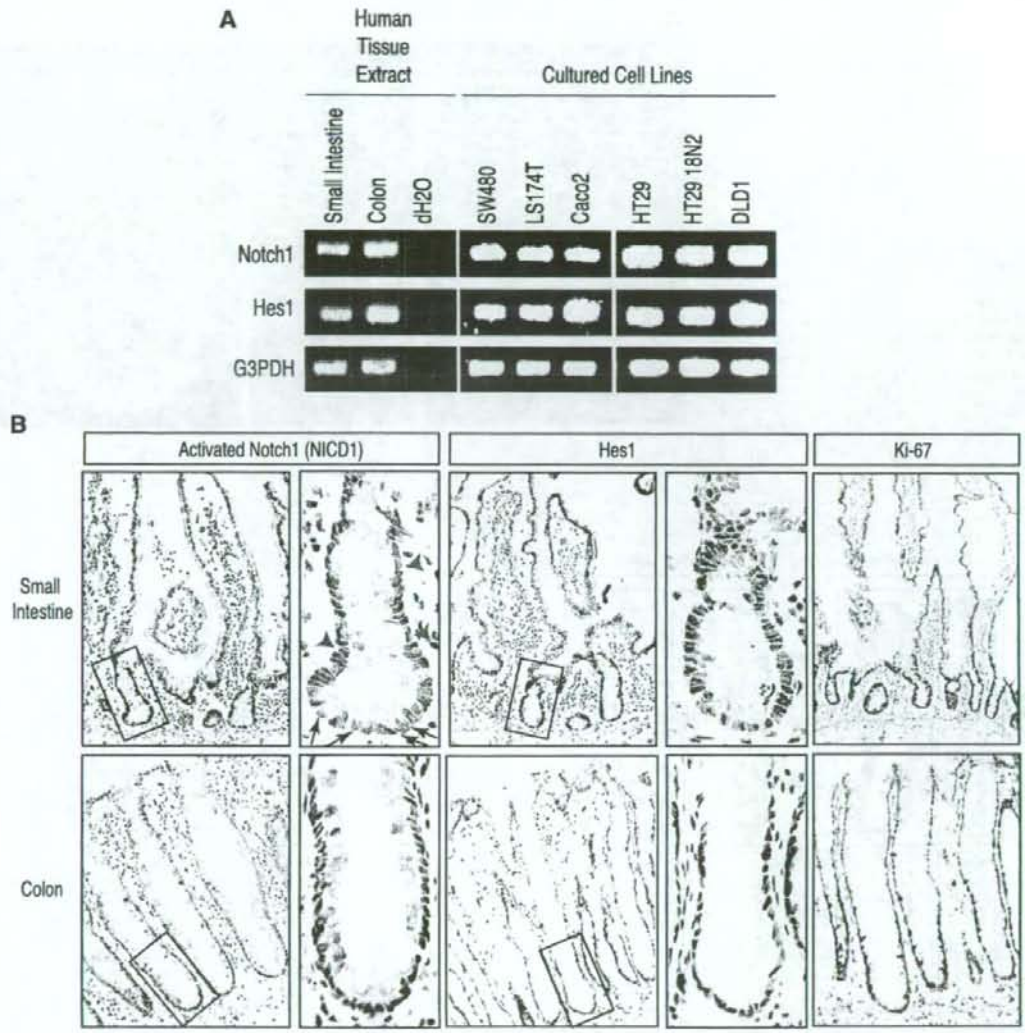

Fig. 6. Notch signaling is activated in crypt epithelial cells of the human intestine. *A*: RT-PCR analysis of human intestinal tissues and human intestinal epithelial cell lines. Expression of both Notch1 and Hes1 are clearly detected in all the examined tissues and cell lines. *B*: immunostaining of human intestinal tissues showing expression of NICD1, Hes1, and Ki-67. Brown staining with DAB showed positive results for NICD1, Hes1, and Ki-67 (original magnification ×200). Magnified view of the squared area is shown in the right side of the original picture (original magnification ×1000). Black arrows show Paneth cells clearly containing granules in the cytoplasm showing positive staining for NICD1, whereas red arrowheads show goblet-shaped cells lacking NICD1 staining.

UC. A quantitative analysis revealed that the number of IECs expressing NICD1 or Ki-67 per crypt is significantly increased, whereas the number of IECs producing mucin is significantly decreased in the crypts of UC (Fig. 8*B*).

We also looked for IECs expressing PLA2G2A within the colonic crypts. There was no expression of PLA2G2A in the crypts of the normal colon (Fig. 9*A*). However, an ectopic expression of PLA2G2A was clearly found in the crypts of the colon epithelia with UC (Fig. 9*B*). Our histological analysis revealed that Notch1 is clearly activated in such IECs ectopically expressing PLA2G2A (Fig. 9, *C* and *D*). Such activation of Notch1 in PLA2G2A-expressing cells could also be found in less inflamed regions of UC where there were fewer PLA2G2A-expressing IECs (Fig. 9, *E* and *F*).

From these results, we confirmed that Notch1 is activated in a greater number of crypt IECs in UC, presumably mediating goblet cell depletion, cell proliferation, and ectopic expression of PLA2G2A. We suggest that such Notch1-mediated changes

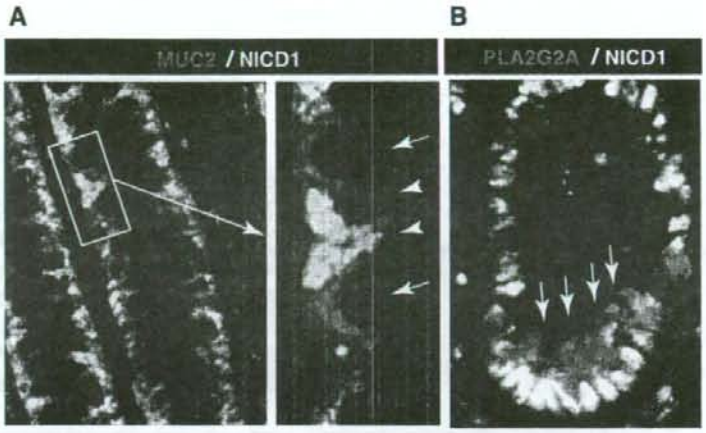

Fig. 7. Human Notch1 is not activated in IECs expressing MUC2 but is activated in IECs expressing PLA2G2A. *A*: human Notch1 was not activated in IECs expressing MUC2 in vivo. Double staining for MUC2 (red) and NICD1 (green) using human colonic tissue is shown. NICD1 and MUC2 were expressed in distinct populations of epithelial cells (*left*, ×400). A magnified view (*right*, ×1600) clearly shows cytoplasmic staining of MUC2 in goblet-shaped cells (yellow arrow), whereas nuclear staining of NICD1 in columnar-shaped cells (white arrowhead). *B*: human Notch1 is activated in IECs expressing PLA2G2A in vivo. Double staining for PLA2G2A (red) and NICD1 (green) using a human small intestinal tissue is shown. NICD1 and PLA2G2A were coexpressed in IECs residing at the lowest part of the crypt, suggesting activation of Notch1 in Paneth cells (yellow arrow, original magnification ×1000).

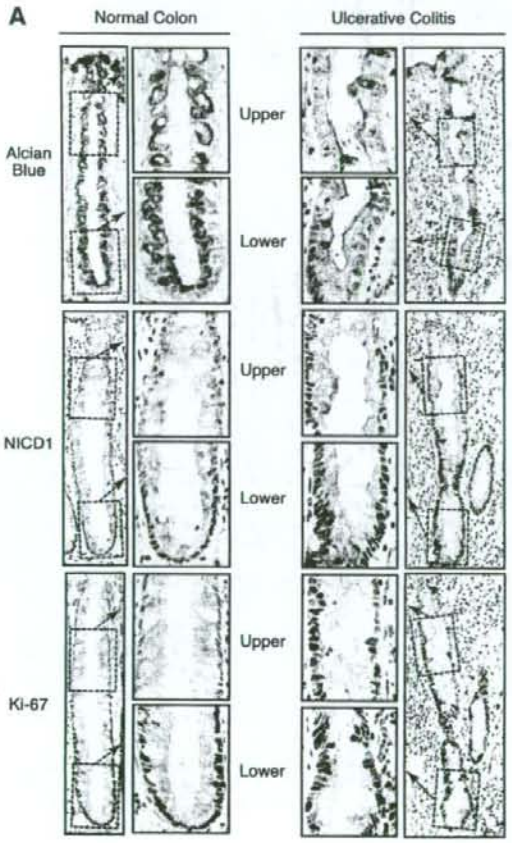

Fig. 8. Increased activation of Notch1 is observed in the crypts of patients with ulcerative colitis (UC). *A*: decreased expression of mucin and increased expression of both NICD1 and Ki-67 were observed in crypts of patients with UC. Mucin expression was examined by Alcian blue staining, whereas expression of NICD1 or Ki-67 was examined by immunohistochemistry with the use of human colonic tissues. Inner column shows magnified view of the upper (Upper) and lower (Lower) crypt areas identified by dashed line in the outer column. A marked decrease in Alcian blue-positive IECs is observed in a crypt of a patient with UC (*top*). In contrast, a marked increase in IECs expressing NICD1 (brown, *middle*) or Ki-67 (brown, *bottom*) was observed in patients with UC. Distribution of IECs expressing NICD1 or Ki-67 was restricted to the lower part of the crypt in normal colon, but it extended to the most upper region of the crypt in UC (original magnification, outer column ×400, inner column ×1600). *B*: significant decrease in IECs expressing mucin and significant increase in IECs expressing NICD1 or Ki-67 were observed in crypts of patients with UC. Quantitative analysis of the histological staining for mucin, NICD1, and Ki-67 is shown. Number of IECs positive for Alcian blue staining or immunohistochemical staining for NICD1 and Ki-67, respectively, were counted per crypt and normalized by total number of IECs. Results are shown as percent positive IECs per crypt. Error bars represent SD. $^*P < 0.05$ on the Student's *t*-test.

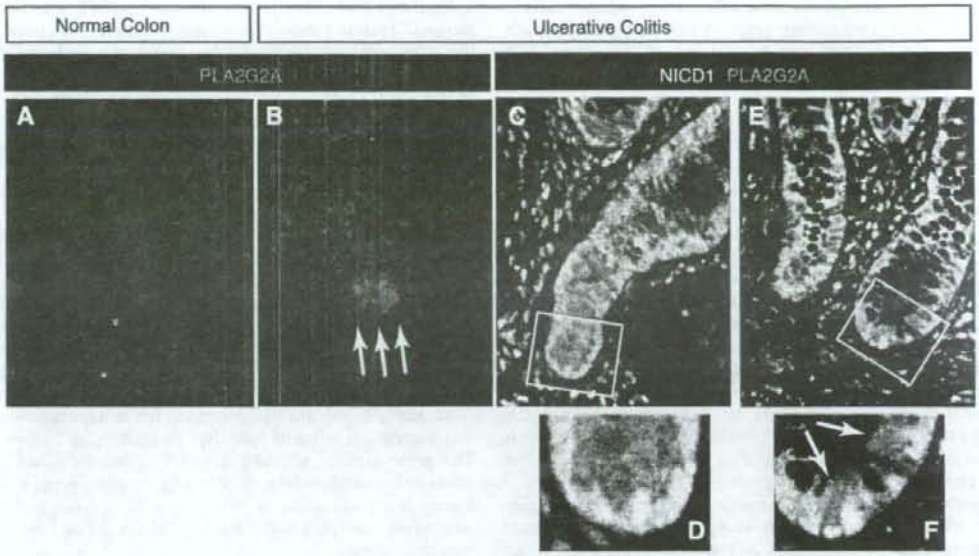

Fig. 9. Notch1 is activated in IECs ectopically expressing PLA2G2A. Fluorescent immunostaining for PLA2G2A (red) was completely negative in the crypts of normal colon (*A*, original magnification ×400), whereas some of the IECs in the crypts of a patient with UC were clearly positive for PLA2G2A (*B*, yellow arrow, original magnification ×400). Some cells in the lamina propria were also positive for PLA2G2A. Double immunostaining for NICD1 (green) and PLA2G2A (red) showed coexpression of NICD1 and PLA2G2A by colonic IECs of a patient with UC (*C–F*). In the inflamed region (*C, D*), NICD1 was expressed in most parts of the crypt IECs, and some proportion of those IECs coexpressed PLA2G2A (*C*, original magnification ×400). A magnified view (*D*, original magnification ×1000) of the indicated region (white square in *C*) clearly showed a nuclear distribution of NICD1 and a cytoplasmic distribution of PLA2G2A. In a less inflamed region, few IECs appeared to be positive for both NICD1 and PLA2G2A (*E*, original magnification ×400). Magnified view of the indicated region (white square in *E*) confirms coexpression of NICD1 and PLA2G2A in the nucleus and cytoplasm of an IEC, respectively (*F*, yellow arrow, original magnification ×1000).

observed in the mucosa of UC are not detrimental changes contributing to the persistence of the disease, but rather they are positive responses that help to regenerate the damaged epithelia, thereby aggressively contributing to the termination and recovery from the disease.

DISCUSSION

To date, several studies using knockout mice have revealed various functions of Notch signaling in IECs; one critical function is that of regulating the cell fates of IECs (31). The recent model accepted in such studies implicates Notch activation as a positive regulator of absorptive cell differentiation but a negative regulator of the differentiation of secretory lineage cells, including goblet cells. However, studies have suggested that Notch activation not only acts to determine the cell fates of progenitor IECs, but it may also regulate the number of proliferating populations within the crypt (6, 28, 33). Our results are consistent with the previous observations, and they further highlight the critical role of Notch activation in a situation when the rapid expansion of IECs is required (e.g., during the regeneration process in UC). Since the in vivo phenotype of Notch inhibition showed not only the loss of absorptive lineage cells but also the loss of the entire epithelial layer, this suggested that the activation of Notch may contribute to the expansion of both absorptive and secretory precursor cells and even stem cells. This is consistent with the observation by Vooijs et al. (34) that IECs that matured into absorptive cells must have also experienced Notch activation during development from the stem cell. Thus our results demonstrated the importance of Notch activation in the expansion of multilineage precursor IECs, whose function becomes critically required when tissue damage is present. In contrast, although Notch activation was predominant in the proliferating IECs of the colitic mucosa, its role in postmitotic IECs might be of less importance (42).

A recent study has shown that the chronic inhibition of Notch activation using LY411,575 (for up to 15 consecutive days) could impair the development of lymphoid cells (14, 36). Thus it may be possible that such an effect of LY411,575 might have altered the local immune function of the DSS-treated mice and thereby exacerbated their colitis. Indeed, LY411,575 proved to have a systemic effect, especially on the development of thymocytes (Supplemental Fig. S1). However, no effect was observed on splenocytes (Supplemental Fig. S1). Also, no effect was observed on local production of proinflammatory cytokines (Supplemental Fig. S2). Thus, although it is possible that LY411,575 might have some effect on the inflammatory response, its involvement on the exacerbation of the present colitis model may be minimal.

Also, GSI has been reported to promote the differentiation and inhibit proliferation of mice intestinal adenoma through the inhibition of Notch activation (33). Therefore, GSIs have been reported to have an antitumor effect (32). However, our results showed that the effects of GSIs may not be specific for tumor